

Fault failure with moderate earthquakes

M.J.S. JOHNSTON¹, A.T. LINDE², M.T. GLADWIN³ and R.D. BORCHERDT¹

¹ U.S. Geological Survey, 345 Middlefield Road, Menlo Park, CA 94025 (U.S.A.)

² D.T.M., Carnegie Institution of Washington, Washington, D.C. (U.S.A.)

³ University of Queensland, Brisbane, Qld. (Australia)

(Received January 27, 1986; revised version accepted May 8, 1986.)

Abstract

Johnston, M.J.S., Linde, A.T., Gladwin, M.T. and Borchardt, R.D., 1987. Fault failure with moderate earthquakes. In: R.L. Wesson (Editor), *Mechanics of Earthquake Faulting*. *Tectonophysics*, 144: 189–206.

High resolution strain and tilt recordings were made in the near-field of, and prior to, the May 1983 Coalinga earthquake ($M_L = 6.7$, $\Delta = 51$ km), the August 4, 1985, Kettleman Hills earthquake ($M_L = 5.5$, $\Delta = 34$ km), the April 1984 Morgan Hill earthquake ($M_L = 6.1$, $\Delta = 55$ km), the November 1984 Round Valley earthquake ($M_L = 5.8$, $\Delta = 54$ km), the January 14, 1978, Izu, Japan earthquake ($M_L = 7.0$, $\Delta = 28$ km), and several other smaller magnitude earthquakes. These recordings were made with near-surface instruments (resolution 10^{-8}), with borehole dilatometers (resolution 10^{-10}) and a 3-component borehole strainmeter (resolution 10^{-9}). While observed coseismic offsets are generally in good agreement with expectations from elastic dislocation theory, and while post-seismic deformation continued, in some cases, with a moment comparable to that of the main shock, preseismic strain or tilt perturbations from hours to seconds (or less) before the main shock are not apparent above the present resolution. Precursory slip for these events, if any occurred, must have had a moment less than a few percent of that of the main event. To the extent that these records reflect general fault behavior, the strong constraint on the size and amount of slip triggering major rupture makes prediction of the onset times and final magnitudes of the rupture zones a difficult task unless the instruments are fortuitously installed near the rupture initiation point. These data are best explained by an inhomogeneous failure model for which various areas of the fault plane have either different stress-slip constitutive laws or spatially varying constitutive parameters. Other work on seismic waveform analysis and synthetic waveforms indicates that the rupturing process is inhomogeneous and controlled by points of higher strength. These models indicate that rupture initiation occurs at smaller regions of higher strength which, when broken, allow runaway catastrophic failure.

Introduction

Research into the mechanics of fault failure indicates that nonlinear strain precedes rupture and this has provided hope that detection of these strain changes will lead to a method for earthquake prediction. This premise derives from theoretical models (Kostrov, 1966; Andrews, 1976; Richards, 1976; Stuart, 1979; Freund, 1979; Rice and Rudnicki, 1979; Stuart and Mavko, 1979; Das and Scholz, 1981; Rice, 1983; Rundle et al., 1984) and laboratory generated failure of crustal materi-

als (Dieterich, 1979; Mogi, 1981; Mogi et al., 1982) which predict that accelerating deformation will occur before the dynamic slip instability that results in an earthquake.

From model studies and laboratory measurements it is not clear whether the entire eventual rupture zone exhibits nonlinear behavior (as implied by "preparation zone" terminology (Sadovsky et al., 1972) and most simple theoretical models of the rupture process) or whether a small region of higher strength fails and, by drawing upon the elastic strain energy in the region, trig-

gers rupture over a much larger area. If nonlinear (accelerating) deformation occurs over the entire zone of subsequent seismic rupture, arrays of sensitive strain and tilt instruments should readily detect it. The expected signals have an easily identifiable form (nonlinear exponential strain increase) during the period immediately preceding rupture initiation. Also, the total slip moment (preseismic, coseismic and postseismic) could be determined when each phase of the rupture process is identified. On the other hand, if failure initiates in small regions of high strength and expands to any arbitrary size until stopped by another mechanical or geometrically strong barrier, detection of preseismic slip and, more importantly, prediction of the final rupture size, would be difficult to achieve (Brune, 1979).

The time scale of failure is also not clear, although the absence of obvious tidal triggering (Heaton, 1982) implies that the final stage of failure occurs at periods comparable to, or shorter than, the major earth tidal periods (12.42, 23.93 and 25.82 h, etc). Numerous observations (Rikitake, 1976; Mogi, 1985) indicate cases when this appears to be true. The shortest time scale for nonlinear strain can be estimated from subcritical crack growth in brittle materials (Atkinson, 1979). However, it is expected that the presence of fluids

would stabilize and slow down the process of cascading crack fusion in rock at the temperatures and pressures expected in the upper 10 km of the earth's crust (Rice and Rudnicki, 1979). This would imply a time scale of about 1 s or longer. If the time scale is between 1 s and 1 day, continuous measurements of the state of strain and tilt in the earth's crust near moderate to large earthquakes should quickly provide detailed information on time history, failure mechanics, and size (moment) of the prerupture failure provided these measurements are taken at a high enough sensitivity during the last few hours to seconds before rupture occurs.

Observations of crustal strain at high sensitivity near large earthquakes during the final stages before rupture are unfortunately rare, and knowledge of the time scale and mechanics of failure is therefore limited. This results largely from the infrequency of earthquakes and the poor areal coverage with adequate instrumentation. With the installation of borehole strain and tilt arrays along the San Andreas fault system (Fig. 1) and in other seismically active places during the last 10 years, data is now being accumulated. Along the San Andreas fault, six events have occurred for which we have near-field recordings at high sensitivity. These events are the Coalinga earthquake ($M_L =$

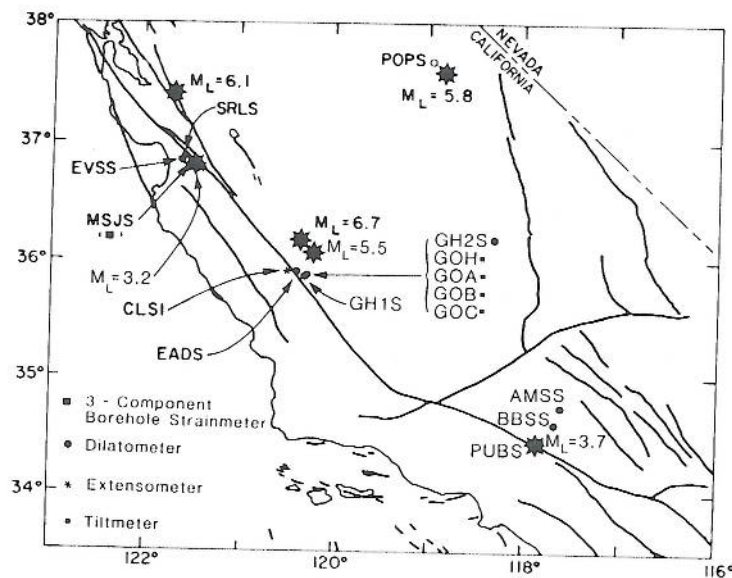


Fig. 1. Borehole crustal strain and tilt sites in California and moderate earthquakes (discussed in the text) recorded at these sites.

6.7) on May 2, 1983, the Kettleman Hills earthquake ($M_L = 5.5$) of August 4, 1985, the Round Valley earthquake ($M_L = 5.8$), on November 23, 1984, the Morgan Hill earthquake ($M_L = 6.1$), on April 24, 1984, the San Juan Bautista earthquake ($M_L = 3.2$), on May 26, 1984, and the Punchbowl earthquake ($M_L = 3.7$) on October 31, 1985. In addition, we have investigated the data from similar instruments, as presented by Sacks et al. (1979), for the Izu-Oshima earthquake ($M_L = 7.0$) on January 14, 1978. In this paper we use these 7 sets of data firstly, to document the state of strain during the last few hours to the last few seconds before each earthquake and to discuss how these observations compare with theory. Secondly, we estimate the maximum likely preseismic slip moment in each case, as a fraction of the observed seismic moment. Thirdly, the observed coseismic strain offsets from the deep borehole instruments are compared with that calculated from simple elastic dislocation models of the events. Finally, some details of postseismic strains are discussed.

It should be pointed out that, in terms of earthquake prediction terminology, the time duration discussed here relates to "short term prediction" (Rikitake, 1976). We will not be discussing any longer term strain changes or redistribution of strain energy in the region before any of these earthquakes.

Theoretical models and laboratory observations

It is now generally accepted that failure in an earthquake rupture zone is a nonlinear process in which the slip velocity accelerates exponentially towards sonic levels. Theoretical models of this process have focused initially on understanding and synthetically generating the dynamic displacement, velocity and acceleration fields of earthquakes by modelling them as propagating cracks in an elastic medium (Kostrov, 1966; Andrews, 1976; Richards, 1976; Das and Scholz, 1981). Recently, a more general approach has evolved in which instability criteria are introduced in the region by choice of particular constitutive properties with or without the presence of pore fluids (Stuart, 1979; Freund, 1979; Rice and Rudnicki, 1979; Stuart and Mavko, 1979; Dmowska and Li,

1982; Rice, 1983; Rundle et al., 1984). Irrespective of the modelling technique, displacement (strain) in the failure region is expected to increase exponentially with time until seismic radiation is generated. Figure 2 shows an example from the crack model of an earthquake proposed by Das and Scholz (1981) showing the crack radius as a function of time as failure is approached.

Coupling of deformation and pore fluid diffusion may partly stabilize the zone but the nonlinear characteristics remain. Figure 3 shows the normalized strain time history for the instability model of Rice and Rudnicki (1979) in which an ellipsoidal inclusion with constitutive properties which are uniform but different from those in the surrounding fluid-filled medium, is strained until instability occurs. The effect of fluid coupling causes the instability to occur in a more gradual manner than for a similar model with no fluid (Fig. 3) with the time scale controlled by fluid diffusion rather than by the nonlinear mechanical properties of rock (Rice and Rudnicki, 1979). Strain during the final stages before failure accelerates dramatically in comparison with earlier periods with maximum strain occurring, as expected, at the point of rupture.

Laboratory experiments also indicate that these last stages of failure of crustal rock (sometimes termed tertiary creep) are the end result of a process of cascading crack coalescence which results in strain time histories similar to those shown

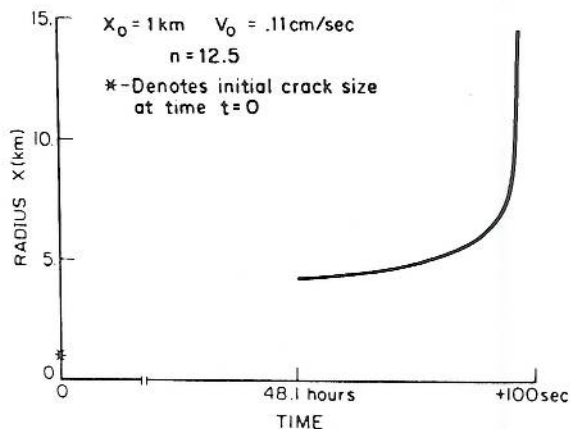


Fig. 2. Rupture geometry as a function of time before failure for a simple crack model of crustal failure (after Das and Scholz, 1981).

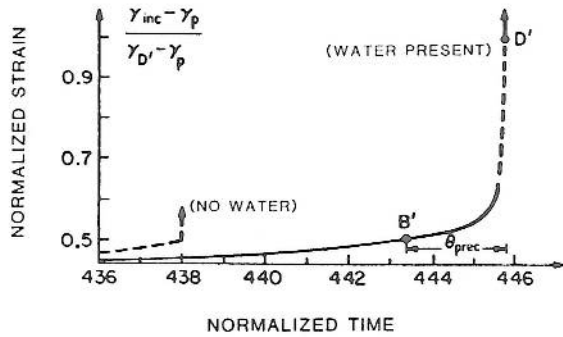


Fig. 3. Normalized strain time history arising from fault instability models with and without the presence of water (from Rice and Rudnicki, 1979). θ_{prec} refers to the precursor time defined by Rice and Rudnicki (1979).

in Figs. 2 and 3 (see for example Mogi, 1985). Large-scale laboratory models with artificial faults, either containing or without gouge material, show similar behavior (Dieterich, 1979; Mogi, 1981; Mogi et al., 1982; Mogi, 1985).

The general form of the failure curves (Figs. 2 and 3) has provided a basis of hope in earthquake research that surface detection of subsurface failure would occur with a time scale (precursor time) that could provide useful warning of the impending rupture (Rice and Rudnicki, 1979). Furthermore, detection of this rapid deformation preceding earthquakes could provide discernible estimates of mechanical properties within the failing zone.

Some of the clearest and perhaps diagnostic signals related to the earthquake source process are expected on sensitive strain instrumentation therefore during the period leading up to the generation of seismic radiation (usually termed the earthquake "origin time"). We note that the observed deformation at ground surface should be similar in form to the time histories in Figs. 2 and 3 but will scale with distance, and may be superimposed on signals resulting from longer term strain redistribution in the region. For recordings in the near-field of earthquakes (i.e., within a few rupture lengths) the maximum strain signals would be expected before the first P-wave arrival depending on how directly the strain is coupled.

Summary of observations

The earthquakes for which we have near-field observations during the final stages of failure are listed in Table 1 and, except for the Izu-Oshima earthquake, are plotted in Fig. 1. Also listed in Table 1 are the detailed locations, occurrence times, depths, magnitudes, seismically determined moments and the maximum possible moment release, as discussed below, during the immediate preseismic period. The five largest earthquakes are as follows:

Coalinga earthquake

The Coalinga earthquake ($M_L = 6.7$) (Fig. 4) occurred at 23 42 h (UT) on May 2, 1983, on a W-dipping low-angle thrust fault about 35 km east of the San Andreas fault near the town of Coalinga. The earthquake had a moment of 6×10^{25} dyne-cm, a dip of 67° down to the southeast, a strike of N53W, and a 20 km by 10 km aftershock zone (Eaton, 1985a). During the last few hours to seconds before the earthquake, three shallow borehole tiltmeters were operating at the Gold Hill site near Parkfield (GOH, GOA and GOB) (3 m deep—see Johnston and Mortensen, 1974 for instrument description), and one strainmeter (10 m in length with a N-S orientation—see Johnston et al., 1977 for instrument description), was operating at Middle Mountain (CLS1). Each tiltmeter had a N-S and an E-W tilt component capable of resolving tilt perturbations of $0.01 \mu\text{rad}$. The data are recorded in analog form on a Rustrak recorder (chart speed = 1.3 cm/hr with output recorded every 4 s) and with digital telemetry (10 min sample rate with least count = $0.01 \mu\text{rad}$). The strainmeter is a 10 m invar extensometer with a differential capacitance transducer capable of resolving a few nanostrain (least count = $0.002 \mu\text{strain}$).

The analog records from the 3 tiltmeters and the N-S component of the strainmeter, with the sections of the record during the last few minutes photographically enlarged, are shown in Figs. 5a-d. The main features of these records are: (1) the uneventful character of the data during the few hours, the last few minutes, and, in most

TABLE 1

Earthquake parameters for events discussed in the text taken, in order, from Eaton (1984, 1985a, 1985b), Johnston et al. (1986), L. Jones (pers. commun.), R. Lester (pers. commun.) and Shimazaki and Somerville (1978). Also included are estimates of the maximum preseismic moment that could have been released in the last few minutes before the earthquake.

Earthquake	Location		Origin time (UT)	Depth (km)	Dip	Strike	Magni- tude	Moment (dyne-cm)	Possible precursive moment (dyne-cm)
	lat.	long.							
Coalinga	36°13.96'N	120°18.6'W	23 42 May 2, 1983	10	67°SE	N53W	6.7	6×10^{25}	1×10^{24}
Kettleman Hills	36°8.63'N	120°9.2'W	12 02 Aug. 4, 1985	11.9	12°SE	N52W	5.5	1.2×10^{25}	7.2×10^{22}
Morgan Hill	37°19.02'N	121°40.9'W	21 15 Apr. 24, 1984	7	84°SW	N33W	6.1	2×10^{25}	1.3×10^{23}
San Juan Bautista	36°50.02'N	121°32.6'W	15 42 May 26, 1984	2.7	90°	N53W	3.2	6.3×10^{20}	1.5×10^{19}
Punchbowl	34°27.7'N	117°53.0'W	19 55 Oct. 31, 1985	7	50°NE	N50W	3.7	6.4×10^{20}	?
Round Valley	37°27.8'N	118°36.5'W	18 08 Nov. 23, 1984	13	85°SE	N30E	5.8	4.8×10^{24}	1.1×10^{23}
Izu, Japan	34°46.1'N	139°12.4'E	12 24 Jan. 14, 1978	4.3	85°N	N90W	7.0	1.1×10^{26}	3.3×10^{24}

cases, within 4 s or less before the earthquake (an exception is the unexplained minor offset in CLS1 (Fig. 5d), about 20 min before the earthquake); (2) the rapid strain and tilt oscillations corresponding to the arrival of the P- and S-seismic strain and tilt waves; (3) offsets in the records at about the

arrival time of the S-wave; and (4) decaying post-seismic signals with an exponential like waveform and a decay time constant between 10 and 30 min.

Greater strain and tilt resolution but poorer temporal resolution is obtained with the data transmitted to Menlo Park by digital telemetry. Figure 6 shows the time histories from the various components for a few hours before the earthquake. Earth tides have been predicted and removed from the records so smaller amplitude signals might be identified. The saw tooth residual in the record reflects least count noise at this time in the digital telemetry.

Kettleman Hills earthquake

An earthquake of $M_L = 5.5$ occurred beneath the western edge of the Great Valley in California at almost 12 02 h on August 4, 1985 (Eaton, 1985b). This event was on a SW-dipping thrust fault near the Kettleman Hills about 17 km southeast of the epicenter of the Coalinga earthquake (Fig. 4). During this period of time, 3 borehole dilatometers (installed between 100 and 200 m—see Sacks et al., 1971 for instrument description), several tiltmeters and the single component

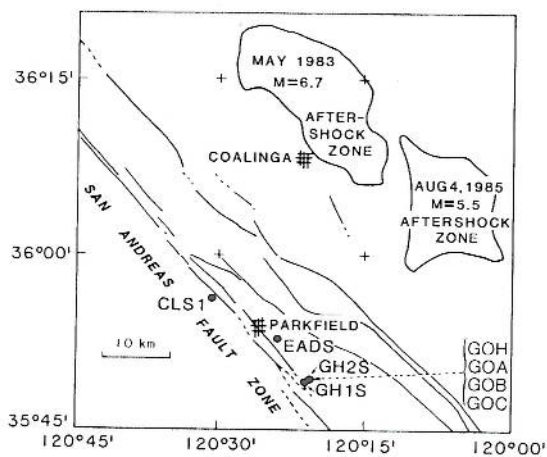


Fig. 4. Location of the dilational strainmeters (EADS, GH1S and GH2S), extensometer (CLS1), and tiltmeters (GOA, GOB, and GOC) with respect to the May 2, 1983, Coalinga earthquake and the August 4, 1985, Kettleman Hills earthquakes and their aftershocks.

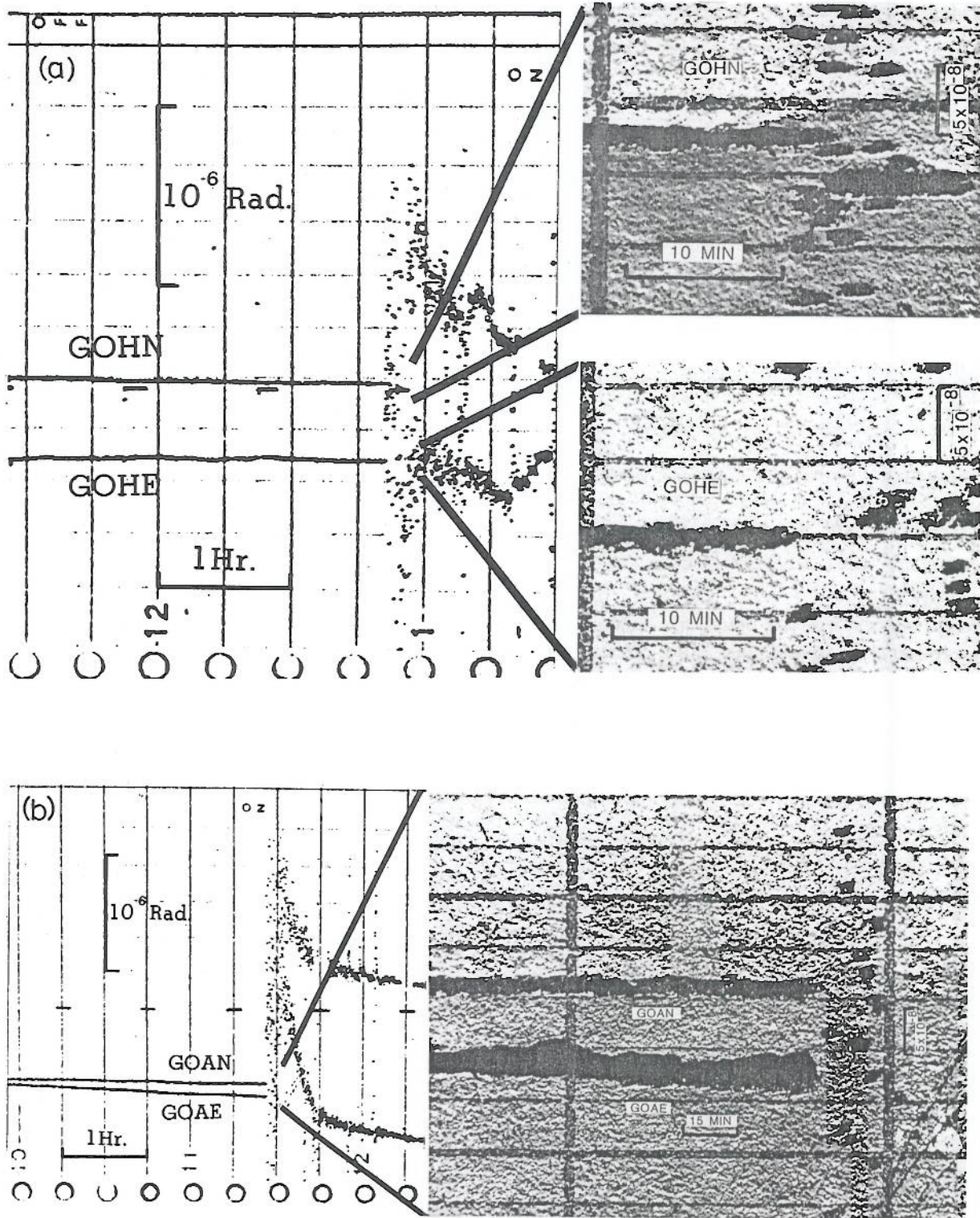
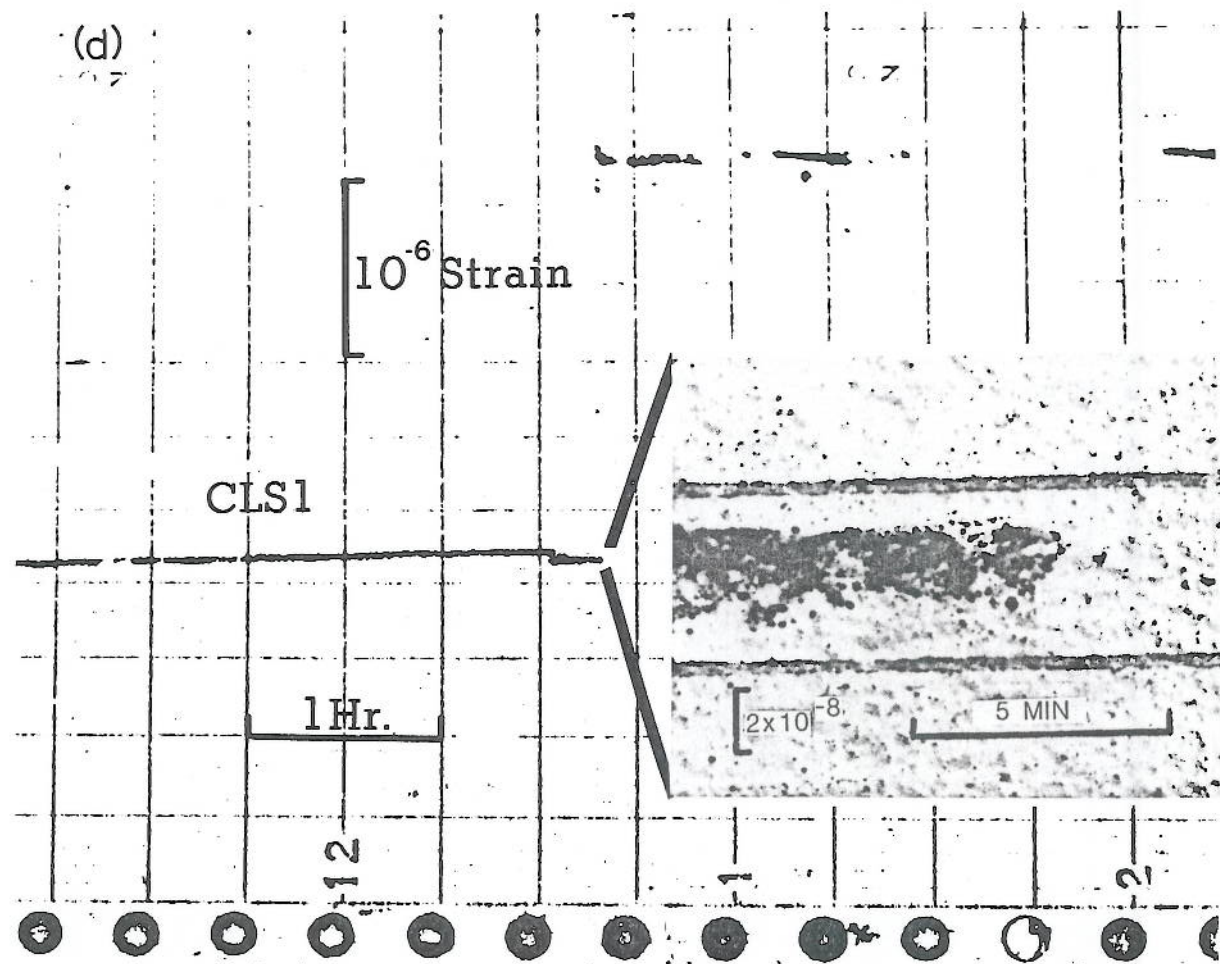
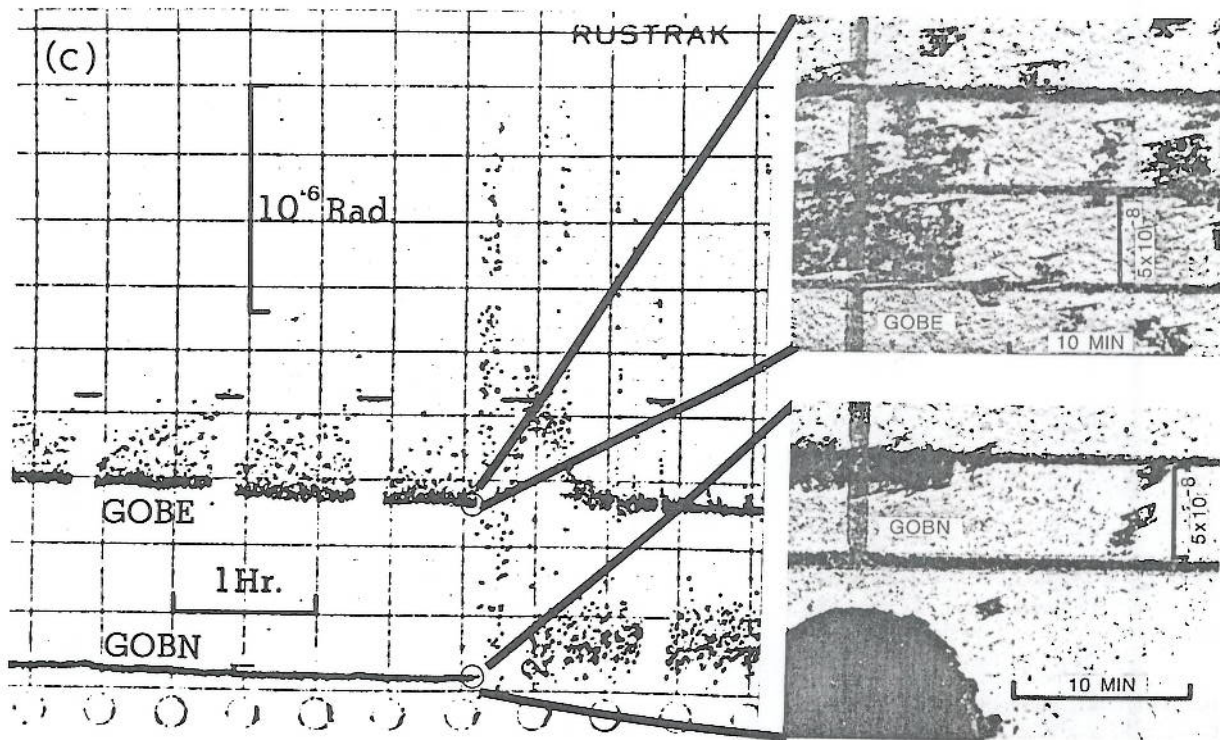


Fig. 5. On-site analog tilt records during the few hours prior to and following the May 1983 Coalinga earthquake with expanded sections showing the few minutes to seconds before and after the earthquake. a. GOH. b. GOA. c. GOB. (Note the recorder noise above the trace for GOBE). d. CLS1.



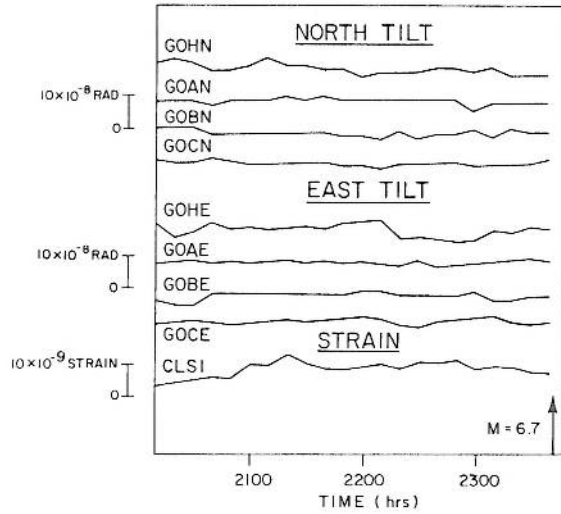


Fig. 6. Tilt and strain data from GOH, GOA, GOB, GOC and CLS1 for a few hours before the May 1983 Coalinga earthquake.

extensometer, were operating at distances between 35 and 38 km from the epicenter. By comparison, the earthquake rupture length is about 20 km (Eaton, 1985b). Strains of less than 10^{-9} can be resolved at short periods on analog recorders connected to the dilatometers (chart speed = 1.25 cm/h with output recorded every 4 s). Only one representative record will be shown here. Figure 7 shows the on-site record from the dilatometer EADS during the few hours before and after the earthquake. Records from the other two dilatometers are similar in form, with the amplitudes of the offsets (see below and Table 2) as expected from simple models of the earthquake.

The longer period oscillations are due to the solid earth tides. The only obvious earthquake related features are the coseismic strain offset, and the dynamic straingram associated with the arrival of the seismic waves. There is no obvious post-seismic strain signal.

Morgan Hill earthquake

The April 24, 1984, Morgan Hill earthquake ($M_L = 6.1$) occurred 50–55 km from several continuously recording strainmeters in the San Juan Bautista region of the San Andreas fault (Fig. 8). The instruments include one 3-component borehole strainmeter MSJS (resolution 10^{-9} with an installation depth of 146 m—see Gladwin, 1984 for a description of the instrument) and two borehole dilatometers, SRLS and EVSS (installation depths of 138 and 118 m respectively). The earthquake occurred at 21 15 h UT at $37^\circ 18.56' N$ and $121^\circ 40.74' W$. It ruptured in a SW-direction, generally towards the strainmeters for a distance of about 30 km between the depths of 4 and 10 km, with a rupture displacement and a moment of 42 ± 4 cm and 2×10^{25} dyne-cm respectively (Eaton, 1984).

Analog records from the dilatometer SRLS are shown in Fig. 9. The recording speed is again 1.25 cm/h and the pen marks the paper every 4 s. Records (obtained at an 18 min sampling interval) from the 3-component strainmeter MSJS for the few days before and after the earthquake are shown in Fig. 10. The components are in direc-

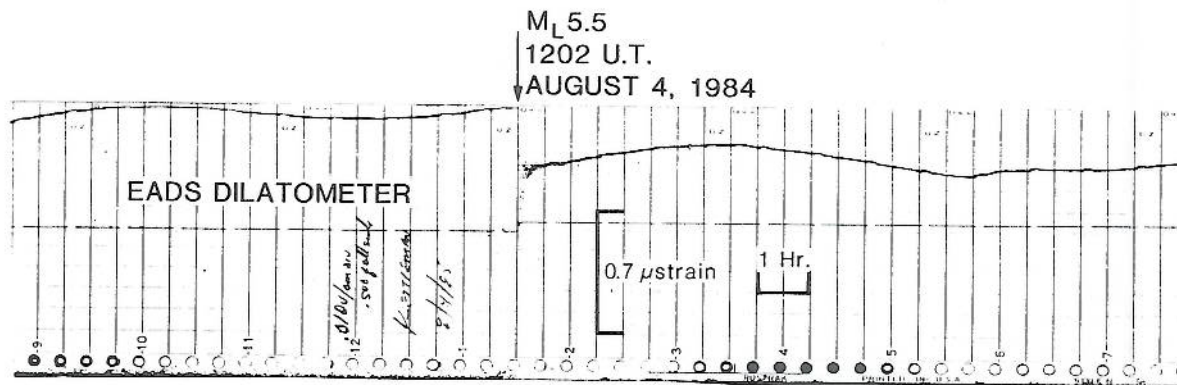


Fig. 7. On-site analog strain records from borehole dilational strainmeter EADS during the few hours prior to and following the August 4, 1985, Kettleman Hills earthquake.

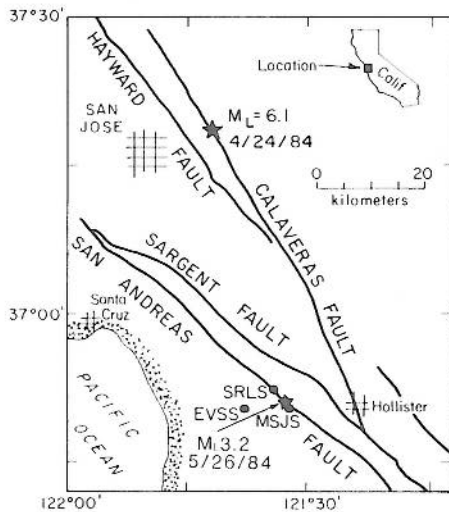


Fig. 8. Location of borehole dilational strainmeters EVSS, SRLS and borehole 3-component strainmeter MSJS with respect to the April 24, 1984, Morgan Hill earthquake. Also shown is the location of an earthquake ($M_L = 3.2$) that occurred on the San Andreas fault on May 26, about a month following the Morgan Hill earthquake.

tions 35° , 95° and 155° west of north. The most interesting features of these records are the absence of preseismic strain changes, the clear coseismic strains and the clear indications of postseismic strain for several hours after the earthquake, particularly on the component MSJS3. Except for the data from EVSS (see below), the

coseismic strains are as expected from simple models of the earthquake. Because of the slow sampling rate, the dynamic straingram is not evident on this record.

San Juan Bautista earthquake

An earthquake of $M_L = 3.2$ occurred at 15 42 h UT on May 26, 1984 at a hypocentral distance of 3.2 km from a dilatometer SRLS, shown in Fig. 8. The data were recorded on a 16-bit digital recorder at a sample rate of 50 Hz with the least count equal to 5×10^{-11} (Borchardt et al., 1985). This earthquake is much smaller than the others discussed above but, because of its proximity to the strainmeter and the high sensitivity of the recordings, it is one of our best near-field records (Johnston et al., 1986).

The data during the few seconds before, to about 10 s after the event are shown in Fig. 11. In this case, there are again no indications of preseismic strain changes. The dynamic straingram is clearly recorded and there is a clear coseismic offset but no obvious postseismic signals. The approximate occurrence time of the earthquake is shown by an arrow. Data for this event are clearly uneventful at the resolution level until the first P-wave arrival. A coseismic offset of 1.86 nanostrain is complete at about the time of arrival of the converted phases of the S-wave.

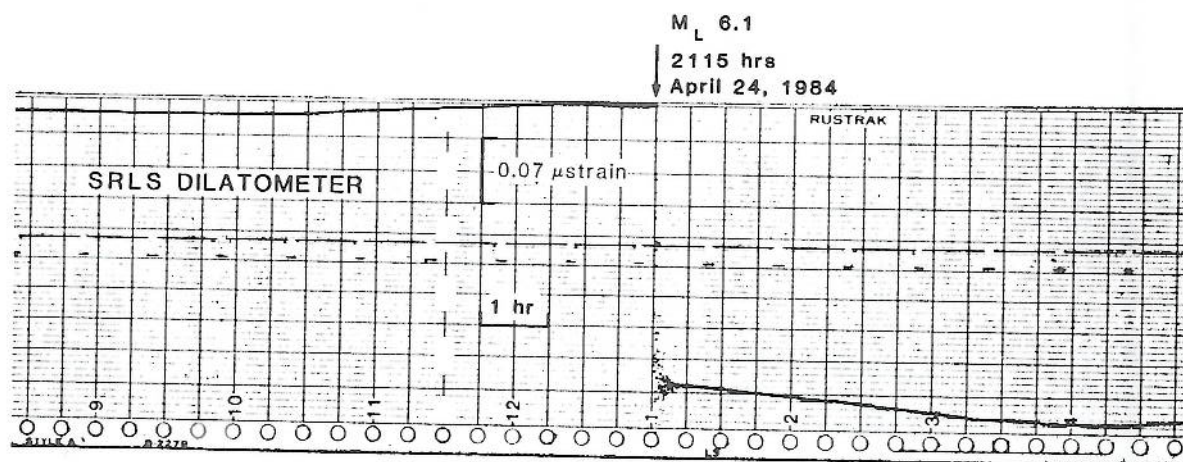


Fig. 9. On-site analog records from borehole dilational strainmeter SRLS during the few hours prior to the April 24, 1984, Morgan Hill earthquake.

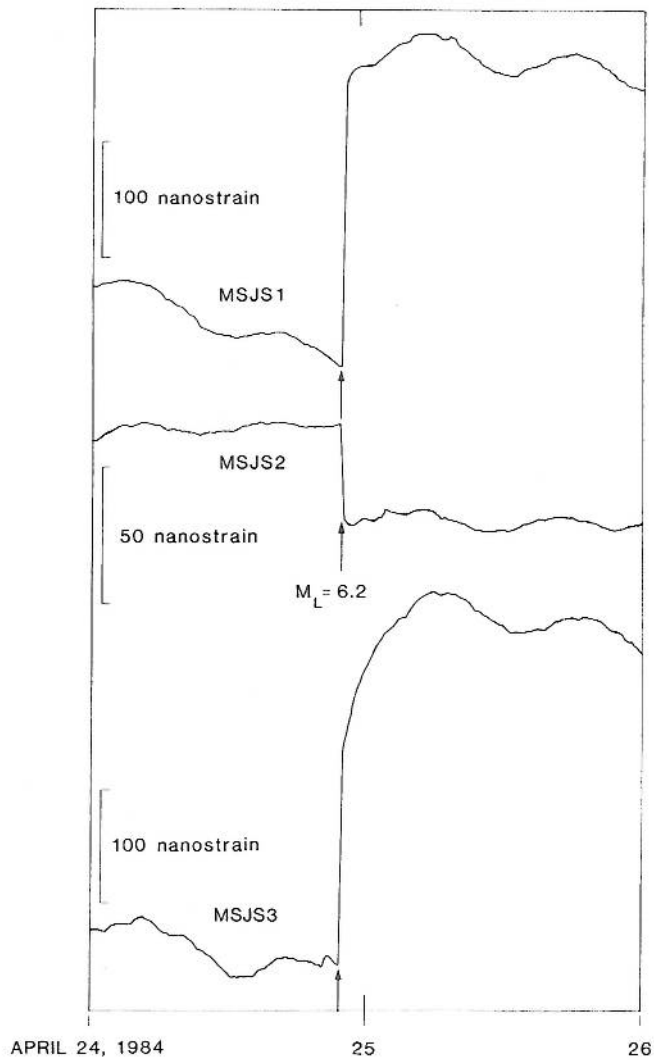


Fig. 10. Telemetered 3-component strain records from the strainmeter MSJS during the 24 h before and after the Morgan Hill earthquake.

Punchbowl earthquake

An earthquake of $M_L = 3.7$ occurred on October 31, 1985, about 7.1 km beneath the dilatometer PUBS (Fig. 12). This instrument is installed at a depth of 186 m. While this event is not as large as some of the other events discussed thus far, it is of interest, firstly because it was almost directly beneath the strainmeter and secondly, because it was recorded at high gain and high sampling rate on a 16-bit digital recorder (Borcherdt et al., 1985). In this case, strains of less than 10^{-11} can be resolved over the period range 0.02–20 s. The data recorded during the period 4 s before, to 14 s after the event are shown in Fig. 13. An expanded version of the 4 s preceding the arrival of the P-wave with an arrow showing the approximate occurrence time of the earthquake is also shown on Fig. 13. The maximum strain changes during these 4 s are not more than 0.2 nanostrain. In contrast, the peak to peak dynamic strains with the earthquake exceed 340 nanostrain. Postseismic strains are not apparent in these records or in longer term records (not shown here) spanning this event.

Round Valley earthquake

During the current sequence of seismic activity in the volcanically active region near Long Valley, California, an earthquake of $M_L = 5.8$ occurred on November 23, 1984, at a distance of 54 km from the borehole dilatometer POPS (Fig. 1). This

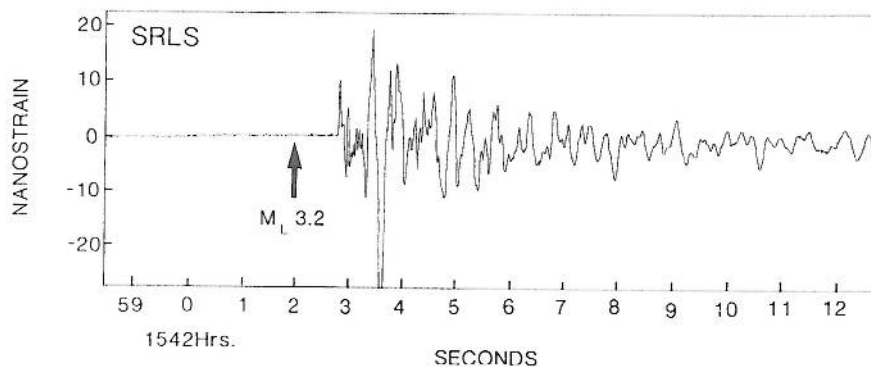


Fig. 11. Digital strain records taken at a hypocentral distance of 3.2 km with a 50 Hz sampling rate during the earthquake ($M_L = 3.2$) at 15 42 on May 26, 1984. The approximate occurrence time of the earthquake is shown with an arrow.

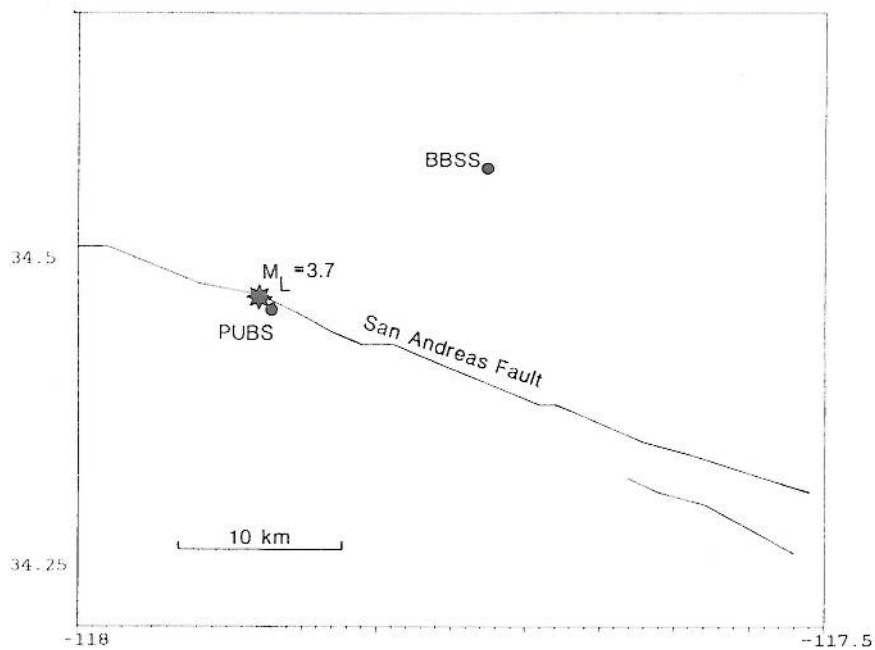


Fig. 12. Location of borehole strainmeters PUBS and BBSS in relation to the earthquake ($M_L = 3.7$) at 19 55 h UT on October 31, 1985. The closest strainmeter, PUBS, is 7.1 km from the hypocenter.

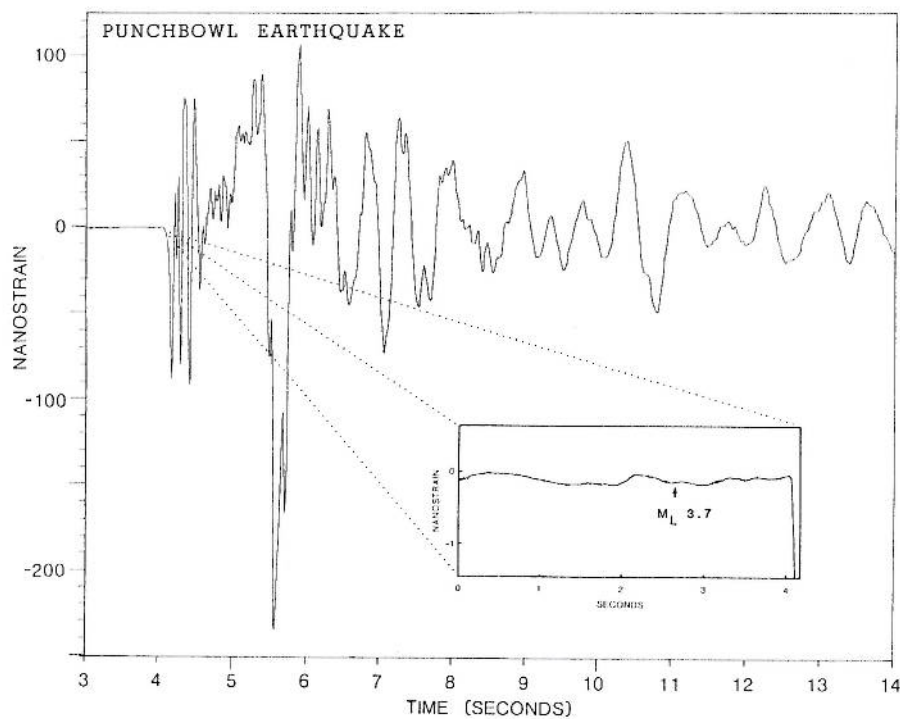


Fig. 13. Strain records during the few seconds before and after the Punchbowl earthquake ($M_L = 3.7$) on October 31, 1985. The expanded section shows the record during the 4 s before the first P-wave arrival. The approximate occurrence time of the earthquake is shown with an arrow.

instrument is installed at a depth of 162 m just on the west side of the caldera. On-site recordings of this event with the section during the last $\frac{1}{2}$ h before the earthquake, photographically expanded, are shown in Fig. 14. The most curious features of this record are the small strain transient about 15 min before the event, the clear coseismic offset and the unusual postseismic strain response during the few hours following the event. The strain transient is not apparent at this time in other tilt or water level records obtained much closer to the earthquake. The transient therefore appears not to have the earthquake source as its origin. Since this is the only event in a volcanic region for which we have recorded coseismic strains, the degree to which this record might reflect different tectonic behavior or, in the case of the postseismic signal, the effects of seismic waves on the hydrological regime in a volcanic area, is not at all clear. Except for the early strain transient, this is similar in general form to that obtained, for example, during the 1983 Coalinga earthquake (Fig. 5) in that there are no clear indications of accelerating strain during the final minutes to seconds before the event. High gain

digital recorder were not yet installed at this site when the event occurred.

The 1978 Izu-Oshima earthquake, Japan

It is important to question whether these results are characteristic only of the generally shallow strike-slip earthquakes observed on the San Andreas fault, or whether similar results are observed elsewhere. Unfortunately, only a few good quality strain recordings have been obtained in the near-field of moderate earthquakes in other seismically active areas. One example was obtained during the 1978 Izu-Oshima earthquake and reported by Sacks et al., (1979).

This earthquake ($M_L = 7.0$) occurred on January 14, 1978, under the sea between Oshima Island and the Izu Peninsula. Before and during the 1978 Izu earthquake, 3 Sacks-Evertson dilational strainmeters were operating at distances comparable to the subsequent source length from the event. The location of these sites and the aftershock zone is shown in Fig. 15 (taken from Sacks et al., 1979). The record sections during the last few hours, including enlarged sections during

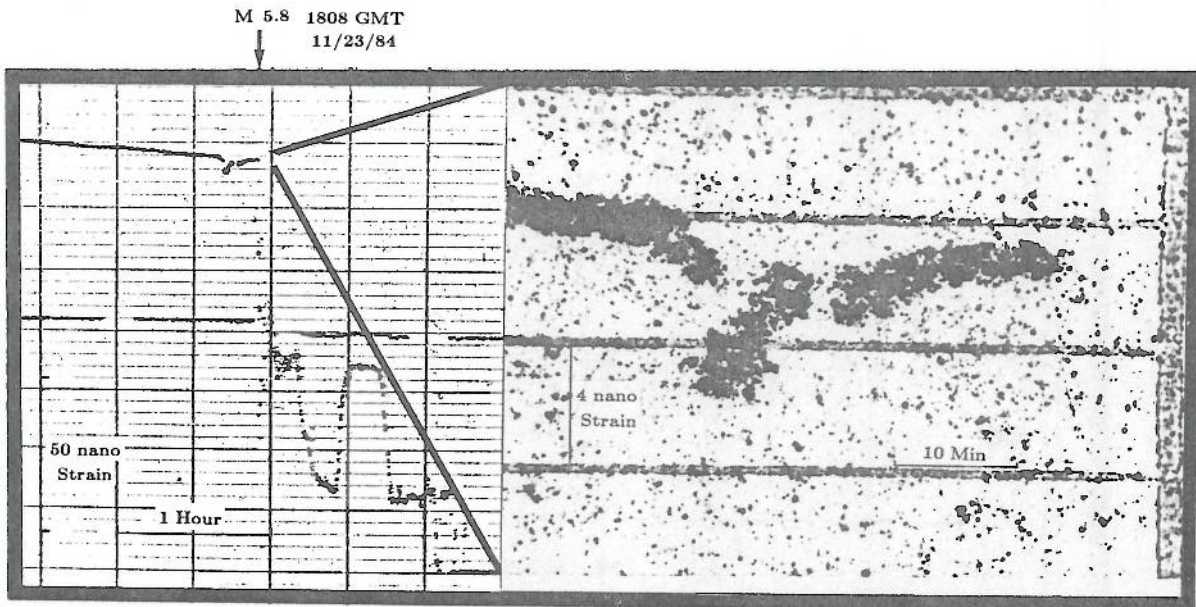


Fig. 14. On-site analog records from borehole dilational strainmeter POPS during the few hours prior to the November 23, 1984, Round Valley earthquake with expanded sections showing the last few minutes to few seconds before and after the earthquake.

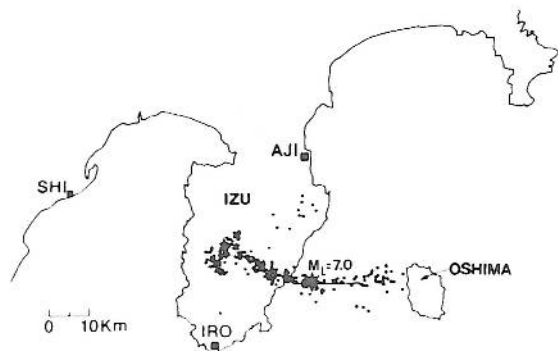


Fig. 15. Location of dilational strainmeters near the 1978, Izu, Japan earthquake and its aftershocks (after Sacks et al., 1979).

the last few minutes are shown in Fig. 16. Because of filtering, the high-frequency straingram is not evident in the record. The main features observed during the several earthquakes on the San Andreas fault are evident here. The biggest difference is the amplitude of the postseismic signals seen on all of the instruments which Sacks et al. (1979) have argued, results from aseismic slippage on several other faults in the region following the earthquake

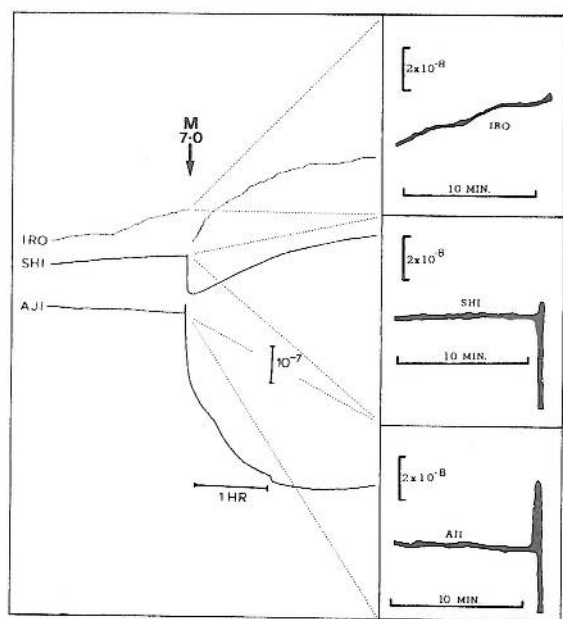


Fig. 16. On-site analog records from borehole dilational strainmeters IRO, SHI, and AJI during the few hours prior to and following the Izu, Japan, earthquake with expanded sections during the last 10 min (after Sacks et al., 1979).

of $M_L = 7.0$. Also, this earthquake was preceded by longer term anomalous strain changes lasting several weeks.

Discussion

For each of these 7 earthquakes it is clear that, if changes in tilt and strain occurred during the immediate preseismic phase (i.e. during the last few hours to seconds before these events), these changes must have been small compared with the dynamic and static strains or tilts associated with each earthquake. In all but one case, there are no indications of dramatically accelerating strain rates until the first P-wave arrival at the instrument. In the single exceptional case, a strain anomaly about 15 min prior to the Round Valley earthquake is unexplained but is not of the exponentially accelerating form that might be expected from precursory failure models. There are no clear indications of substantial strain redistribution around the eventual rupture surface immediately prior to rupture or extraction of significant elastic strain energy from the system.

The data for each earthquake can be used to estimate the maximum possible preseismic moment for each event by assuming that the preseismic strain signals are right at the level of resolution of the instruments and then calculating the moment at the earthquake hypocenter that would generate strains or tilts at the instruments with these amplitudes. The preseismic moment determined in this way can then be compared with the subsequent earthquake moment. For example, in the case of the Morgan Hill earthquake, the maximum strain transient that could have occurred at SRLS in the last few seconds before rupture is about 1 nanostrain (Fig. 9). In the last few hours, this could not have been more than a few nanostrain. The maximum moment release on the eventual rupture plane that would generate strains of no more than 2 nanostrain at SRLS is then estimated from a simple finite size dislocation model of the earthquake such as described by Press (1965) or Okada (1985). The moment in this case, is 1.3×10^{23} dyne-cm. In contrast, the seismic moment of the earthquake is 2×10^{25} dyne-cm.

Estimates of the maximum likely preseismic

moments were made for each of the earthquakes considered here. These are listed in Table 1 with the seismic moments of the earthquakes. These preseismic moments (expressed as a percentage of the seismic moment) are also plotted in Fig. 17 against the seismic moment. From this figure it is clear that the most optimistic estimates of the preseismic moment are not more than a percent or so of the seismic moment of the earthquakes. The higher estimates, for example for the Coalinga earthquake, reflect the poorer signal resolution at that time.

While it seems unlikely that both the wealth of laboratory data on anelastic deformation of crustal rocks as failure is approached, and theoretical calculations on crack initiation and crack behavior are not somehow relevant to initiation of fault failure, it is clear, at least for these examples, that slip instability over the entire subsequent fault rupture will not explain these data without requiring an unrealistically short time constant for rupture initiation or extremely small prerupture deformation. Laboratory measurements of crustal rocks under high confining pressure indicate that anelastic strains before failure are comparable to the elastic strain release upon failure (Jaeger and Cook, 1976). The scale on which rupture initiates is apparently not that of the subsequent earthquake. If so, the fault model relevant to this

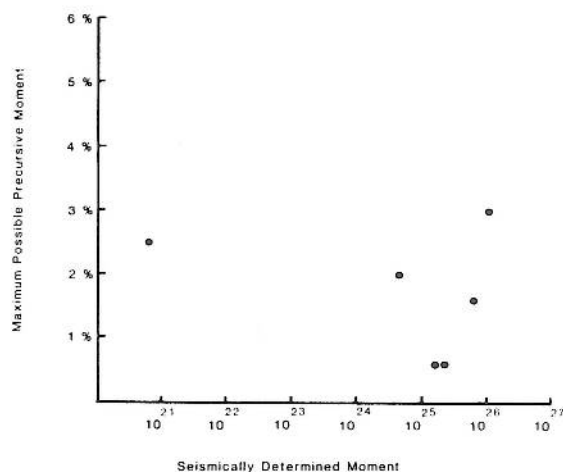


Fig. 17. Plot of maximum possible prerupture moment as a percentage of the seismically determined moment for the studied events listed in Table 1.

process must be inhomogeneous in character to accommodate these observations. That is, crustal failure does not occur simultaneously across the entire rupture zone but is apparently triggered by failure of small localized zones.

That an inhomogeneous faulting model be suggested to describe the initiation of failure is not at all surprising. Wyss and Brune (1967) and many researchers since then have made similar suggestions. Based on careful analysis of seismic waveforms and on synthetic waveform generation Kanamori (1981) and Lay et al. (1982), have shown that an inhomogeneous rupture model is required to explain the complex waveforms generated by many large earthquakes. These data have been used to suggest that regions of greater strength (barriers or asperities) can be broken during fault failure and energy release from these regions contributes to the seismic radiation.

Inhomogeneous fault models have been proposed by McGarr (1981) to explain peak ground motion in an earthquake, by Dieterich (1986) to explain simulated faulting in laboratory samples, and, in a more general way, by Rundle et al. (1984) to explain seismicity gaps, fault roughness indicated by complex seismic waveforms, and apparent triggering effects. The data reported here are consistent with the suggestion outlined above that rupture initiation most likely occurs at smaller regions of higher strength which, when broken, allow runaway catastrophic failure. An inhomogeneous failure model, such as that proposed by Rundle et al. (1984), for which various areas of the fault plane have different stress-slip constitutive laws appears necessary therefore, to explain the processes that lead to failure as well as those that occur following failure. Other inhomogeneous failure models are also possible.

The coseismic observations can be separated into two parts, the dynamic straingram and the static strain field offset generated by the earthquake. Theory of the strain seismogram is the subject of a different paper and will not be pursued further here. The observation of strain offsets from earthquakes has a long history. Early hopes that these offsets could be observed teleseismically (Press, 1965) have not been realized. The primary reason seems to have been that tilt and strain

observations recorded under conditions of high acceleration in the cracked and fractured near-surface material in tunnels, caves and shallow boreholes, are not reliable because the materials and coupling are not stable (McHugh and Johnston, 1977). Installation of instruments in expansive cement in deep boreholes appears to have solved this problem (Sacks et al., 1971, 1979). With the network of deep borehole instruments along the San Andreas fault, we have data which indicate that coseismic strain steps can be recorded reliably.

For most of the events shown here, clear strain offsets have been recorded. Each of these offsets can be compared with that expected from the simplest model of each corresponding earthquake. These elastic dislocation models (Press, 1965; Okada, 1985) assume that the moment of the earthquake is generated by uniform slip over the eventual rupture plane, which is assumed to be indicated by the aftershock zone. An example of such a simple dislocation model for the August 4, 1985, Kettleman Hills earthquake is shown in Fig. 18. In this case, the seismically determined moment is 1.2×10^{25} dyne-cm, the aftershock zone measures 20 by 15 km at a depth of 12 km, with a dip of 12° down to the southwest and a strike of N52W. For these dimensions, and assuming a shear modulus of 3×10^5 bar, the slip expected

MODEL OF KETTLEMAN HILLS EARTHQUAKE ($M_1 = 5.5$) AUGUST 4, 1984

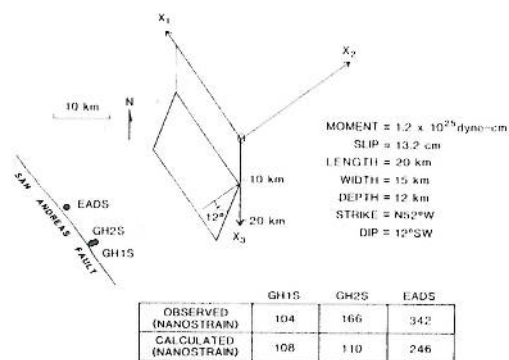


Fig. 18. Example of dislocation model used to calculate strain offsets from a finite size rupture dimension (generally estimated from the aftershock distribution) and the seismically determined moment, dip and strike. The techniques used follow Press (1965). In this case we show the simple dislocation model of the August 4, 1985, Kettleman Hills earthquake.

TABLE 2

Observed and calculated strain steps on borehole strainmeters for the earthquakes studied.

Earthquake	Instrument	Observed coseismic steps (nanostrain)	Calculated coseismic steps (nanostrain)
Kettleman Hills	GH1S	104	108
Kettleman Hills	GH2S	166	110
Kettleman Hills	EADS	342	246
Morgan Hill	MSJ1	242	233
Morgan Hill	MSJ2	-34	-30
Morgan Hill	MSJ3	192	111
Morgan Hill	SRLS	-304	-325
Morgan Hill	EVSS	-33?	-143
San Juan Bautista	SRLS	1.86	1.1
Round Valley	POPS	64.6	43

for the earthquake is about 13 cm. The observed and calculated strain offsets for the 3 borehole instruments in the area are listed.

Similar models were generated for each of the other earthquakes for which we have strain offsets recorded. The calculated and the observed offsets are listed in Table 2 and are plotted in Fig. 19. The observed and calculated offsets are in good general agreement except for one example (marked with "?") recorded on the instrument EVSS. Because this instrument was installed just above a large fracture zone, nonlinear effects caused by the accelerations from the seismic waves are more likely to be significant.

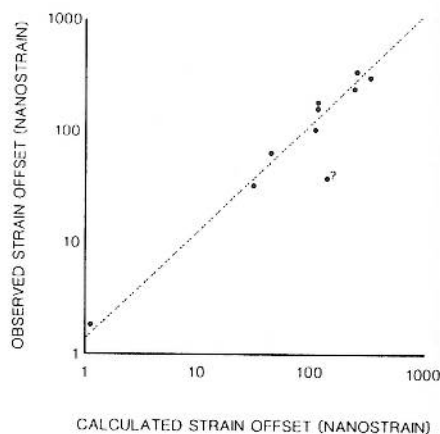


Fig. 19. Observed coseismic strain offsets as a function of calculated offsets from simple dislocation models of the earthquakes. See text for comments on point labelled with "?".

STRAIN & TILT	PRE-SEISMIC	CO-SEISMIC	POST-SEISMIC
EXPECTED (Models)			?
ACTUAL (Data)			
AGREEMENT	POOR	GOOD	

Fig. 20. Cartoon showing the general features of the expected and observed prerupture, corupture and postrupture strain signals for the events studied.

Postseismic responses observed in these data are quite variable. Some of these effects may be due to afterslip, or triggered slip on other faults, as suggested by Sacks et al. (1979), to explain postseismic changes following the 1978 Izu, Japan, earthquake. Others may result from aquifer system response to the incoming seismic waves. In this case, the time constant will be determined by the diffusion time constant. This appears to be generally true for measurements taken near the water table (McHugh and Johnston, 1977). While the clearest postseismic strain signals have been observed on instruments near the creeping sections of the San Andreas fault for only the larger earthquakes (Coalinga, Morgan Hill), and in Long Valley, for the Round Valley earthquake, the data are still too few to suggest a pattern. The pre-seismic, coseismic, and postseismic strain behavior for these events in comparison with expected behavior is summarized in cartoon form in Fig. 20.

Conclusions

We have attempted to detect preseismic strain change near several recent moderate earthquakes during the final hours to seconds approaching rupture. If preseismic strain changes occur they are below the present instrument resolution (typically $\approx 10^{-9}$) and are insignificant compared with the dynamic straingram and static strain offsets. In the cases investigated, the maximum possible moment of preseismic rupture appears to be not

more than a few percent of the final seismic or geodetic moment. Because of the geometry involved, an even smaller preseismic moment is indicated if this moment were distributed across the entire final rupture area. Laboratory data indicate that such a small ratio of preseismic slip (or deformation) to coseismic slip is unlikely (Dietrich, 1981).

These data are most easily explained by an inhomogeneous faulting model for which different areas of the fault plane have either different constitutive properties or different stress-slip constitutive laws such as proposed by Rundle et al. (1984) and indicated by observations of complex seismic waveform generation during rupture (Kanamori, 1981; Lay et al., 1982). For these inhomogeneous models, failure initiation occurs in relatively localized zones and expands until barriers of sufficient strength to stop the rupture are encountered. The processes that lead to failure as well as those that follow failure are inhomogeneous in character. Energy driving the system appears to come from uniformly accumulated elastic strain energy (Prescott et al., 1979).

Analogies might be made to a variety of small-scale initiation processes triggering large-scale energy release (e.g., avalanches, explosions, failure of brittle materials, etc). An essential point as regards prediction of the occurrence times of these moderate earthquakes is that this will be a difficult task unless the monitoring instruments are sufficiently close to the initiation zone to detect the onset of instability. If this is the case, it is easy to understand why some earthquakes have detectable short term precursors, as discussed by Rikitake (1976), and others apparently do not. For very large events, preseismic changes may be comparable with the seismic event (Rikitake, 1976; Sacks et al., 1978).

Coseismic offsets in the static strain field changes generated by these earthquakes appear to be explained by relatively simple models. The variable and generally amplified coseismic offset response to earthquakes previously observed in the cracked and fractured material near the earth's surface, and in caves or tunnels, appears to be avoided by installing instruments in grout, in deep boreholes.

A variety of postseismic responses were observed for these events. This may reflect either continuing afterslip following the earthquake or equilibration of the fluid regime, or a combination of both. Afterslip is common in regions where aseismic fault slip occurs, such as on the San Andreas fault following the 1966 Parkfield earthquake (Smith and Wyss, 1968), and on the Imperial fault following the 1979 Imperial Valley earthquake (Langbein et al., 1983).

Acknowledgements

Collection of these data results from the sustained field efforts of G.D. Myren, A.C. Jones, C.E. Mortensen and many others. Alan Jones provided the careful photographic enlargement of the on-site analog records. Gary Glassmoyer, John Watson, Chris Dietel and others helped with the GEOS data retrieval and Rick Lester and Lucy Jones provided the seismologically determined parameters from network data for the various events. Two of us (A.L. and M.G.) were partially supported by separate grants (14-08-0001-G-960 and 14-08-0001-22025) from the U.S.G.S. Earthquake Hazard Reduction Program.

References

- Andrews, D.J., 1976. Rupture velocity of plain-strain shear cracks. *J. Geophys. Res.*, 81: 5679–5687.
- Atkinson, B.K., 1979. A fracture mechanics study of subcritical tensile cracking of quartz in wet environments. *Pure Appl. Geophys.*, 117: 1011–1024.
- Borcherdt, R.D., Fletcher, J.B., Jensen, E.G., Maxwell, G.L., Van Schaack, J.R., Warrick, R.E., Cranswick, E., Johnston, M.J.S. and McClearn, R., 1985. A General Earth Observation System (GEOS). *Bull. Seismol. Soc. Am.*, 75: 1783–1826.
- Brune, J.N., 1979. Implications of earthquake triggering and rupture propagation for earthquake prediction based on premonitory phenomena. *J. Geophys. Res.*, 84: 2195–2198.
- Das, S. and Scholz, C.H., 1981. Theory of time-dependent rupture in the earth. *J. Geophys. Res.*, 86: 6039–6051.
- Dieterich, J.H., 1978. Modeling of rock friction I. Experimental results and constitutive equations. *J. Geophys. Res.*, 84: 2161–2168.
- Dieterich, J.H., 1981. Constitutive properties of faults with simulated gouge. *Geophys. Monogr., Am. Geophys. Union, (J. Handin Festschrift)*, 24: 103–120.
- Dieterich, J.H., 1986. A model for the nucleation of earthquake slip. In: *Earthquake Source Mechanics*. Am. Geophys. Union, Monogr., 37: 37–47.
- Dmowska, R. and Li, V.C., 1982. A mechanical model of precursory source processes for some large earthquakes. *Geophys. Res. Lett.*, 9: 393–396.
- Eaton, J.P., 1984. Location, focal mechanism, and magnitude of the Morgan Hill earthquake derived from CALNET records. U.S. Geol. Surv. Open-file Rep., 84-498: 10–17.
- Eaton, J.P., 1985a. Regional seismic background of the May 2, 1983, Coalinga earthquake. U.S. Geol. Surv. Open-file Rep., 85-44: 44–60.
- Eaton, J.P., 1985b. The North Kettleman Hills earthquake of August 4, 1985, and its first week of after-shocks—a preliminary report (unpublished).
- Freund, L.B., 1979. The mechanics of dynamic shear crack propagation. *J. Geophys. Res.*, 84: 2199–2209.
- Gladwin, M.T., 1984. High precision multi-component bore-hole deformation monitoring. *Rev. Sci. Instrum.*, 55: 2011–2016.
- Heaton, T.H., 1982. Tidal triggering of earthquakes. *Bull. Seismol. Soc. Am.*, 72: 2181–2200.
- Jaeger, J.C. and Cook, N.G.W., 1976. *Fundamentals of Rock Mechanics*. Wiley, New York, 585 pp.
- Johnston, M.J.S. and Mortensen, C.E., 1974. Tilt precursors before earthquakes on the San Andreas fault, California. *Science*, 186: 1031–1034.
- Johnston, M.J.S., Jones, A.C. and Daul, W., 1976. Continuous strain measurements during and preceding episodic creep on the San Andreas fault. *J. Geophys. Res.*, 82: 5683–5691.
- Johnston, M.J.S., Borcherdt, R.D. and Linde, A.T., 1986. Short period strain ($0.1-10^5$ s): Near source strain field for an earthquake (M_L 3.2) near San Juan Bautista, California. *J. Geophys. Res.*, 91: 11,947–11,502.
- Kanamori, H., 1981. The nature of seismicity patterns before major earthquakes. In: D.W. Simpson and P.G. Richards (Editors), *Earthquake Prediction, an International Review (Maurice Ewing Series, Vol. IV)*. Am. Geophys. Union, Washington, D.C., pp. 1–19.
- Kostrov, B.V., 1966. Unsteady propagation of longitudinal shear cracks. *J. Appl. Math. Mech. (U.S.S.R.)*, 30: 1241–1248.
- Langbein, J., McGarr, A., Johnston, M.J.S. and Harsh, P.W., 1983. Geodetic measurements of postseismic crustal deformation following the 1979 Imperial Valley earthquake, California. *Bull. Seismol. Soc. Am.*, 73: 1203–1224.
- Lay, T., Kanamori, H. and Ruff, L., 1982. The asperity model and the nature of large subduction zone earthquakes. *Earthquake Predict. Res.*, 1: 3–71.
- McHugh, S. and Johnston, M.J.S., 1977. An analysis of coseismic tilt changes from an array in central California. *J. Geophys. Res.*, 82: 5692–5698.
- McGarr, A., Sacks, I.S., Linde, A.T., Spottiswood, S.M. and Green, R.W.E., 1982. Coseismic and other short term strain changes recorded with Sacks-Evertson strainmeters in a deep mine, South Africa. *Geophys. J.R. Astron. Soc.*, 70: 717–740.
- McGarr, A., 1981. Analysis of peak ground motion in terms of a model of inhomogeneous faulting. *J. Geophys. Res.*, 86: 3901–3912.

- Mogi, K., 1981. Earthquake prediction and rock mechanics. *J. Soc. Mater. Sci. Jpn.*, 30: 105-118.
- Mogi, K., 1985. *Earthquake Prediction*. Academic Press, New York, 255 pp.
- Mogi, K., Yoshikawa, S. and Kogita, S., 1982. Changes preceding the sudden slip of artificial fault planes (2)—precursory deformation. *Abstr. Seismol. Soc. Jpn.*, 1: 128.
- Okada, Y., 1985. Surface Deformation due to shear and tensile faults in a half-space. *Bull. Seismol. Soc. Am.*, 75: 1135-1154.
- Prescott, W.H., Savage, J.C. and Kinoshita, W.T., 1979. Strain accumulation rates in the western United States between 1970 and 1978. *J. Geophys. Res.*, 84: 5423-5435.
- Press, F., 1965. Displacements, strains and tilts at teleseismic distances. *J. Geophys. Res.*, 70: 2395-2412.
- Rice, J.R., 1983. Constitutive relations for fault slip and earthquake instabilities. *Pure Appl. Geophys.*, 121: 443-475.
- Rice, J.R. and Rudnicki, J.W., 1979. Earthquake precursory effects due to pore fluid stabilization of a weakening fault zone. *J. Geophys. Res.*, 84: 2177-2193.
- Richards, P.G., 1976. Dynamic motions near an earthquake fault: A three-dimensional solution. *Bull. Seismol. Soc. Am.*, 65: 93-112.
- Rikitake, T., 1976. *Earthquake Prediction*. Elsevier Amsterdam, 357 pp.
- Rundle, J.B., Kanamori, H. and McNally, K.C., 1984. An inhomogeneous fault model for gaps, asperities, barriers and seismic migration. *J. Geophys. Res.*, 89: 10219-10231.
- Sacks, I.S., Suyehiro, S., Evertson, D.W. and Yamagishi, Y., 1971. Sacks-Evertson strainmeter, its installation in Japan and some preliminary results concerning strain steps. *Pap. Meteorol. and Geophys.*, 22: 195-207.
- Sacks, I.S., Suyehiro, S., Linde, A.T. and Snoke, J.A., 1978. Slow earthquakes and stress redistribution. *Nature*, 275: 599-602.
- Sacks, I.S., Linde, A.T., Snoke, J.A. and Suyehiro, S., 1979. A slow earthquake sequence following the Izu-Oshima earthquake of 1978. In: D.W. Simpson and P.G. Richards (Editors), *Earthquake Prediction, an International Review*. Maurice Ewing Ser., Vol. IV. Am. Geophys. Union, Washington, D.C., pp. 617-628.
- Sadovsky, M.A., Nersesov, I.L., Nigmatullaev, S.K., Latynina, L.A., Lukk, A. A., Semenov, A.N., Simbireva, I.G. and Ulomov, V.I., 1972. The processes preceding strong earthquakes in some regions of Middle Asia. *Tectonophysics*, 14: 295-307.
- Shimazaki, K. and Somerville, P., 1978. Summary of the static and dynamic parameters of Izu-Oshima-Kinkai Earthquake of January 14, 1978. *Bull. Earthquakes Res. Inst.*, 53: 613-628.
- Smith, S.W. and Wyss, M., 1968. Displacement on the San Andreas fault initiated by the 1966 Parkfield earthquake. *Bull. Seismol. Soc. Am.*, 68: 1955-1974.
- Stuart, W.D., 1979. Strain softening prior to two dimensional strike-slip earthquakes. *J. Geophys. Res.*, 84: 1063-1070.
- Stuart, W.D. and Mavko, G., 1979. Earthquake instability on a strike-slip fault. *J. Geophys. Res.*, 84: 2153-2160.
- Wyss, M. and Brune, J., 1967. The Alaskan earthquake of 28 March 1964: A complex multiple rupture. *Bull. Seismol. Soc. Am.*, 57: 1017-1023.